Compression of Packed Particulate Systems: Simulations and Experiments in Graphitic Li-ion Anodes

Y.-B. Yi

C.-W. Wang

Department of Mechanical Engineering,
College of Engineering,
University of Michigan,
Ann Arbor, MI 48109

A. M. Sastry[1]
Department of Mechanical Engineering,
College of Engineering,
University of Michigan,
Ann Arbor, MI 48109 and
Department of Biomedical Engineering,
College of Engineering,
University of Michigan,
Ann Arbor, MI 48109

Increased thermal conductivity, electronic conductivity, and reversible capacity (i.e., reduced irreversible capacity loss, or ICL) have been demonstrably achievable by compression of anodes into higher volume fraction plates, though excessive compression can impair Li-ion battery performance. In our previous study, we correlated conductivity and compression of these materials. Here, we further investigated the effects of friction and deformability of particles on the compressibility of model carbons of Li-ion anodes. First, we implemented a statistically unbiased technique for generating a range of random particulate systems, from permeable to impermeable arrangements, along with a contact model for randomly arranged triaxial ellipsoidal particles, suitable for implementation in finite element analysis of compression of a random, porous system. We then quantified the relationship between interfacial friction and jamming fraction in spherical to ellipsoidal systems and applied these models to correlate maximum stresses and different frictional coefficients, with morphology (obtained by image analysis) of graphite particles in Li-ion anodes. The simulated results were compared with the experiments, showing that the friction coefficient in the system is close to 0.1 and that the applied pressure above 200 kg/cm^2 (200 *MPa*) *can damage the materials in SL-20 electrodes. We also conclude that use of maximum jamming fractions to assess likely configuration of mixtures is unrealistic, at best, in real manufacturing processes. Particles change both their overall shapes and relative orientations during deformation sufficient to alter the composite properties: indeed, it is alteration of properties that motivates post-processing at all. Thus, consideration of material properties, or their estimation post facto, using inverse techniques, is clearly merited in composites having volume fractions of particles near percolation onset.* [DOI: 10.1115/1.2130733]

1 Introduction

Increased thermal conductivity, electronic conductivity, and reversible capacity (i.e., reduced irreversible capacity loss, or ICL) have been demonstrably achievable by compression of anodes into higher volume fraction plates [1,2], though excessive compression can impair Li-ion battery performance [3]. Our present interest is in determining the nature of failure progression resulting from compression in the particulate systems that comprise high power-density battery electrodes.

Specifically, Maleki et al. [1] demonstrated that the thermal conductivity increased from 0.32 to 0.65 $W/m \cdot K$ at room temperature as the compression pressure was increased from 250 to 550 kg/cm^2. Striebel et al. [2] found that compression improved reversible capacity, electronic conductivity, and cyclability. Application of 300 kg/m^2 compression to GDR-6 graphite-additive anodes was found to increase reversible capacity from 240 to 340 mAh/g and reduce ICL from 180 to 90 mAh/g for electrodes without compression. Furthermore, compressed electrodes were cycled up to 20 times, without significant capacity losses, while uncompressed electrodes exhibited capacity fade after a single cycle.

Gnanaraj et al. [3] found, however, that excessive pressing might impair performance. They showed that capacities of graphite electrodes, comprised of 90 wt% KS-6 graphite flakes and 10 wt% PVdF binder, were ordered $C_{\text{unpressed}} > C_{\text{pressed}} > C_{\text{rolled}}$, for unpressed, 5000 kg/cm^{-2} (pressed), and machine rolled electrodes, respectively. Our own group [4] postulated that mechanical failure associated with stress localization resulted in these losses. We studied [4] anodes comprised of three different types of natural graphite, compressed at four levels (0, 100, 200, and 300 kg/cm^2). The natural graphites studied were SL-20, a purified natural graphite produced by Superior Graphite, and GDR-6 and GDR-14 natural graphites having 6 and 14 wt% amorphous carbon coatings and produced by Mitsui Mining. Figures 1(*a*) and 1(*b*) show scanning electron microscope (SEM) images of SL-20 with application of 100 kg/cm^2 pressure. They clearly show severely deformed particles in the transverse direction. These images also suggest that particles are semi-permeable; this is important, since conductivity in compressed systems is strongly affected by percolation onset, which in turn depends upon particle permeability [4]. In our previous study, we correlated conductivity and compression of these materials. Here, we further investigate the effects of friction and deformability of particles on the compressibility of model carbons of Li-ion anodes.

Compression of particulate systems has been widely studied in the context of percolation. Mathematically idealized systems have received the most attention. For example, the maximum densities of perfectly rigid particles have been studied extensively [5,6], as a convenient means of determining a volume fraction immediately preceding material failure, and the effective material properties have been derived [7,8]. Real materials systems, however, exhibit two important features not captured by these idealized models. First, friction among particles alters the so-called jamming fraction: in the limit, infinite friction coefficients trivially produce a

[1]Corresponding author; email: amsastry@umich.edu

Contributed by the Materials Division of ASME for publication in the JOURNAL OF ENGINEERING MATERIALS AND TECHNOLOGY. Manuscript received October 12, 2004; final manuscript received March 17, 2005. Review conducted by Greg Schoeppner.

maximum jamming fraction identical to the percolation point, for rigid particles. Second, deformation of particles under compression results in local material failure in any realistic system, well before the maximum jamming fraction is reached.

We define the following parameters for the discussion that follows: *maximum volume fraction (MVF)* is simply the theoretically highest packing density achievable in a monodisperse system of a given type (e.g., 0.74 for monodisperse face-centered cubic packed spheres [9]), *random close-packing fraction (RCP)* is the maximum density that a large, random collection of spheres can attain (e.g., [6]), and *maximal random jamming fraction (MRJ)* is the volume fraction which minimizes an "order parameter" among all statistically homogeneous and isotropic jammed structures [6]. Our objectives in the present study were fourfold:

1. Implement a statistically unbiased technique for generating a range of random particulate systems, from permeable to impermeable arrangements.
2. Develop and implement a contact model for randomly arranged triaxial ellipsoidal particles, suitable for implementation in finite element analysis of compression of random, porous systems.
3. Quantify the relationship between interfacial friction and jamming fraction in spherical to ellipsoidal systems.
4. Apply these models to correlate maximum stresses and different frictional coefficients, with morphology (obtained by image analysis) of graphite particles in Li-ion anodes.

Our simulation models are based on anodes comprised of natural graphite, pressed to a range of anode densities.

2 Methods

2.1 Generation of Randomly Arranged, Impermeable Triaxial Ellipsoids. Random placement of particles has previously been made for purposes of simulation singly or by combination of two basic techniques: dynamic deployment [10], whereby initial positions of particles are assigned and they are assigned velocities to allow elastic collisions when they meet, and growth algorithms [11,5,12], whereby initial positions for particle center-points are assigned randomly in a space, and particle boundaries are assigned a constant rate of "growth," which involves elastic collisions and is halted when further growth of the particles appears impossible. Classically, so-called "maximal packing fractions" in random systems have been studied using the growth algorithm. We take a somewhat simplified approach here in generating the particles, omitting the growth portion of previous algorithms while retaining a statistically unbiased deployment technique to arrange particles. We extend previous work on axisymmetric particles (spheres [13,14] and spherocylinders [15]) by considering triaxial particles.

The general method is summarized as follows. Particles were initially placed randomly in a cell. Initial overlaps were corrected by placing repulsive force couples at contact points of the particles, following the laws of rigid body dynamics. The algorithm was run until no overlap was detected among particles.

Required derivations follow. For a triaxial ellipsoid defined by its center position $X_0=(x_0,y_0,z_0)$, orientation angles $\Theta=(\theta,\varphi,\gamma)$, and three semi-axis lengths a, b, and c, respectively, motion is assumed in $\Re^3$, with linear velocity $V=(v_x,v_y,v_z)$, and rotational velocity $\dot{\Theta}=(\dot{\theta},\dot{\varphi},\dot{\gamma})$ in the local coordinate system, or $\Omega=(\Omega_x,\Omega_y,\Omega_z)$ in the global coordinate system. An arbitrary point $X=(x,y,z)$ on the surface of such an ellipsoid can be uniquely described by a matrix equation,

$$(X-X_0)^T R^T C R (X-X_0)=1, \tag{1}$$

where C is the characteristic matrix of ellipsoid

$$C=\begin{bmatrix} 1/c^2 & 0 & 0 \\ 0 & 1/b^2 & 0 \\ 0 & 0 & 1/a^2 \end{bmatrix}, \tag{2}$$

and R is a rotation matrix given by

$$R=\begin{bmatrix} R_{11} & R_{12} & R_{13} \\ R_{21} & R_{22} & R_{23} \\ R_{31} & R_{32} & R_{33} \end{bmatrix}=\begin{bmatrix} \cos\gamma\cos\theta\cos\varphi-\sin\varphi\sin\gamma & -\sin\gamma\cos\theta\cos\varphi-\sin\varphi\cos\gamma & \sin\theta\cos\varphi \\ \cos\gamma\cos\theta\sin\varphi+\cos\varphi\sin\gamma & \cos\gamma\cos\varphi-\cos\theta\sin\varphi\sin\gamma & \sin\theta\sin\varphi \\ -\cos\gamma\sin\theta & \sin\theta\sin\gamma & \cos\theta \end{bmatrix}. \tag{3}$$

The extreme points (x,y,z) on the ellipsoidal surface are then given by

$$H=\sqrt{a^2R_{1k}^2+b^2R_{2k}^2+c^2R_{3k}^2},$$

$$\begin{aligned} x-x_0&=\pm\frac{a^2R_{1k}R_{11}+b^2R_{2k}R_{21}+c^2R_{3k}R_{31}}{H}, \\ y-y_0&=\pm\frac{a^2R_{1k}R_{12}+b^2R_{2k}R_{22}+c^2R_{3k}R_{32}}{H}, \\ z-z_0&=\pm\frac{a^2R_{1k}R_{13}+b^2R_{2k}R_{23}+c^2R_{3k}R_{33}}{H}, \end{aligned} \tag{4}$$

where $k=1$, 2, and 3 in the x, y, and z directions, respectively.

Upon collision, rotational and linear velocities of an ellipsoid ranged from Ω to $\Omega+\Delta\Omega$ and V to $V+\Delta V$, respectively. Conservation of energy in the resulting system can be used to solve for the locations and orientations of colliding particles, per

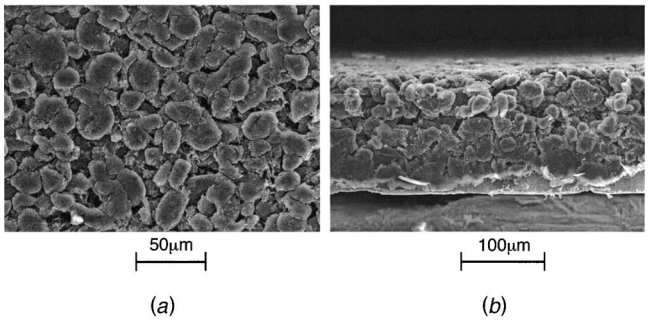

Fig. 1 SEM images of SL-20 anode materials under a pressure of 100 kg/cm^2, including (*a*) a top view and (*b*) a cross-sectional view

$$\Delta\Omega^T I\Omega + \Omega^T I\Delta\Omega + \Delta\Omega^T I\Delta\Omega + \Delta V^T MV + V^T M\Delta V + \Delta V^T M\Delta V = 0, \quad (5)$$

where I is moment of inertia of particle, and M is the mass matrix of particle,

$$M = \frac{4}{3}\pi abc\rho \begin{bmatrix} 1 & 0 & 0 \\ 0 & 1 & 0 \\ 0 & 0 & 1 \end{bmatrix} \quad (6)$$

and ρ is the mass density of the ellipsoids. Let us consider the moment of inertia about the center of mass with rotational axes parallel to the axes of the ellipsoid is

$$\bar{I} = \frac{4}{15}\pi abc\rho \begin{bmatrix} b^2+c^2 & 0 & 0 \\ 0 & a^2+c^2 & 0 \\ 0 & 0 & a^2+b^2 \end{bmatrix}. \quad (7)$$

The moment of inertia I with respect to the global axes can be obtained via the transformation matrix R as

$$I = R^{-1}\bar{I}R. \quad (8)$$

Letting r denote $X-X_0$, and n denote the surface normal at X, balances of linear and angular momentum for an ellipsoid can be written as

$$\vec{r}\times\vec{P} = I\Delta\vec{\Omega} \quad (9)$$

and

$$\vec{P} = M\Delta\vec{V}, \quad (10)$$

respectively, where P is linear momentum induced by the impact force between the ellipsoid and the rigid surface of cell. If we use $T=\vec{r}\times\vec{n}=(r_2n_3-r_3n_2)\vec{i}+(r_3n_1-r_1n_3)\vec{j}+(r_1n_2-r_2n_1)\vec{k}$ and N as the matrix form of the normal, then we can restate the above relations in matrix form as

$$\Delta\Omega = I^{-1}TP, \quad (11)$$

$$\Delta V = M^{-1}NP. \quad (12)$$

Substitution of Eq. (5) yields

$$\Delta\Omega = \frac{-2(N^TV + T^T\Omega)I^{-1}T}{|M^{-1}| + T^TI^{-1}T}. \quad (13)$$

The collision equation between two ellipsoids can be derived similarly from the energy and momentum considerations. We can find that

$$\Delta\Omega_i = \frac{-2(N^T(V_1 - V_2)) + (T_1^T\Omega_1 - T_2^T\Omega_2)}{|M_1^{-1}| + |M_2^{-1}| + (T_1^TI_1^{-1}T_1 + T_2^TI_2^{-1}T_2)} I_i^{-1}T_i, \quad (14)$$

where $i=1,2$ are two distinct particles involved in a single collision.

Iteration in the time domain allows solution for all positions of ellipsoids as

$$R_j(\Theta_j(t+\Delta t)) = R_j(\Omega_j\Delta t)R_j(\Theta_j(t)), \quad (15)$$

$$X_j(t+\Delta t) = X_j(t) + V_j\Delta t, \quad (16)$$

where $j=1,\ldots,n$; n is the total number of particles in the system.

2.2 Implementation of a Contact Model. Explicit contact functions have been derived for specific particles, e.g., identical ellipsoids of revolution [16], and a general molecular dynamics simulation algorithm has been developed for nonspherical particles [17]. Here we present a simplified model in which we set a contact criterion by discretizing the surface of one ellipsoid and successively compared relative positions of grid points with respect to the surface equation of any contacting ellipsoids. These points (given by Eq. (1)) were used to find the contact points between an ellipsoid and the boundary wall.

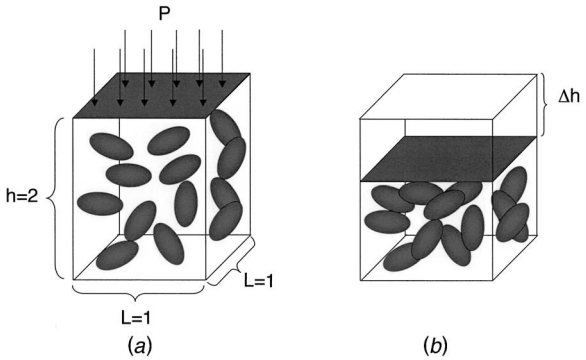

Fig. 2 Schematics of particle compression simulations (*a*) before compression and (*b*) after compression

Finite element meshing of individual particles in the simulations here was performed using FEMLAB© from COMSOL Ltd. Meshes were first created on one particle and then replicated on the others. ABAQUS/EXPLICIT [18] was used to perform the finite element analysis, since it was designed to solve transient dynamics problems involving complex contact interactions among large numbers of independent bodies. The contact pairs were assigned using the "all element based" option to specify self-contact for an all-inclusive element-based surface, instead of exhaustively defining all individual contact pairs required in some other commercial software. The CPU time for running a single simulation on a SUN blade-1500 workstation was ~10–20 h, depending on the spatial arrangement of particles and friction coefficient, etc. The memory consumption was approximately 400 MB on the same computer.

In the Li-ion anode, the graphite particles were initially dispersed in a precursor slurry of 1-methyl-2-pyroolidinone (NMP) and a binder material, poly(vinylidene fluoride) (PVdF) (Kureha 9130) [4,19]. They were then cast onto a Cu foil current collector. Yoo et al. [20] measured the dynamic viscosity of the precursor, which is similar to that used in the anodes studied here, and found that the viscosity of precursor slurry ranges from 0.2 to 5000 $N\cdot s/m^2$ at 1 rad/s, for various synthetic graphites. The viscosity depends upon particle size, packing density, and frequency. The sizes of the SL-20 graphite particles are between 16 and 23 μm [4], and fall within the ranges studied by Yoo et al. [20]; our graphite particles had a density of 2250 kg/m^3 [21].

We conclude then that the shear force due to viscosity is much higher than the force due to gravity; the shear force can be approximated as a friction force as we suggest here. Similarly, the pressure applied after to assure the particle contact is larger than the gravity force acting on each particle. The force acting on the anode particles due to gravity was thus neglected in this study.

2.3 Implementation of a Finite Element Model Incorporating Interfacial Friction. A schematic of the model is shown in Fig. 2. As a first step in the simulation, 500 nonoverlapping particles were generated in a fixed, elastic container, using a rigid body collision algorithm described above. The system size was normalized to $1\times1\times2$ along the x, y, and z directions, respectively. The initial length in the z direction was assumed to be nonunity, such that the whole system at the close packing condition would approximate a unit cube at close packing. The particle size was predetermined in such a way that the initial volume fraction was well below the jamming fraction of rigid particles. The plate was moved at a constant velocity in the vertical z direction, with other boundaries fixed. Each particle was discretized into approximately 300 general-purposed tetrahedron elements and 100 nodes, and therefore the overall size of the problem was about

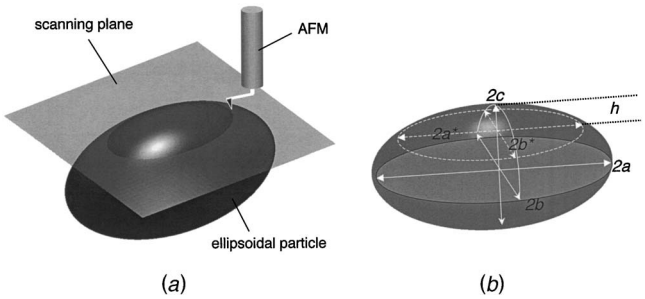

Fig. 3 A schematic showing the reconstruction of ellipsoidal particle geometry using AFM. (*a*) The scanning range covers only a portion of the upper surface, (*b*) geometrical relations among the measured parameters.

150,000 elements with 50,000 nodes. All elements were assigned identical elastic material properties. Linear displacement with respect to time was prescribed.

2.4 Image Analysis of Real Materials. Particles from previously analyzed sample Superior Graphite (SL-20) of compressed natural graphite Li-ion anodes (0, 100, 200, or 300 kg/cm^2) [4,22] were used to inform the models developed here. Pictures shown in Fig. 1 are SEM images of SL-20 anode under pressure of 100 kg/cm^2, illustrating the effect of application of pressure during electrode preparation on an electrode's morphologies at the transverse section. Most particles did not possess axial symmetry, and were approximated as triaxial ellipsoids.

AFM (atomic force microscopy) was used to obtain the required 3D measurements. All pictures were obtained using a NanoScope III Dimension 3000 series BioScope in air-contact mode with Digital Instruments DNP tips. AFM samples were prepared by deposition of a single layer of SL-20 graphite particles onto a glass slide; particles were affixed using double-sided tape. Imaged particles were selected under the optical microscope, because of their alignment in the scanning plane. The maximum scanning range of the AFM in the depth direction is practically only a couple of microns, much smaller than the semi-axis lengths of a graphite particle (>7 μm). Thus, we mapped only a small portion of the upper surface as depicted in Fig. 3. However, we reconstructed the original surface and derived the needed parameters from the properties measured by the following method. Suppose an ellipsoid has semi-axis lengths a, b, and c in the x, y, and z directions, respectively; the projected ellipse of the scanned surface on the x-y plane has semi-axis lengths a^* and b^*, height h, along with the measured mean radii of curvature R_1 and R_2 in the x-z and y-z cross-sectional planes, respectively. Note that the mean curvature of the scanned surface is approximately equal to the curvature at the uppermost point $(0,0,c)$, given by

$$R_1 = \frac{a^2}{c}, \quad R_2 = \frac{b^2}{c}, \tag{17}$$

and the area S of the projected ellipse is

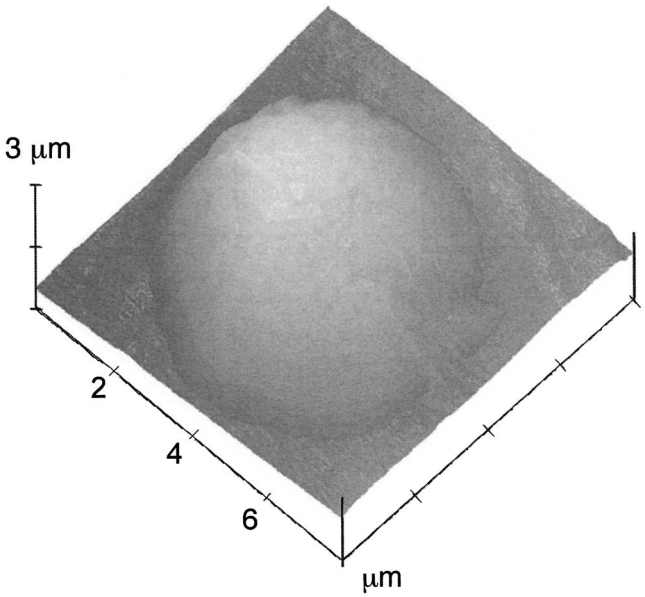

Fig. 4 AFM image on a SL-20 natural graphite particle

$$S = \pi a^* b^* = \pi \sqrt{a^2\left(1 - \frac{(c-h)^2}{c^2}\right) b^2\left(1 - \frac{(c-h)^2}{c^2}\right)}$$
$$= \pi(2hc - c^2)\sqrt{R_1 R_2}. \tag{18}$$

Based on these relations, we solve for a, b, and c. A sample AFM image for a SL-20 natural graphite particle is shown in Fig. 4. Note that in the AFM measurement, a thin layer of the anode material was used as the specimen, and thus the axes of each particle were approximately aligned with the view plane.

3 Results

3.1 Image Analysis and Selection of Model Parameters. The AFM-measured properties for SL-20 natural graphite particles are listed in Table 1.The averaged aspect ratios over all the results are $a/b=1.27$ and $a/c=1.49$ and we use these aspect ratios to construct ellipsoids in the simulation models with the axial lengths listed in Table 2.

The finite element simulation parameters are listed in Table 3. Since simulation results were normalized, material properties were chosen principally based on reduction of time to numerical solution convergence. The parameters listed in Table 3 were found to be an appropriate combination for the transient finite element analysis in terms of the fast convergence speed as well as acceptable tolerance in solution. Briefly, since the study of the dynamic response is beyond the scope of this study, a quasi-static or a long-time solution is preferable as to minimize the inertia effects caused by the motion of the pressing plate. However, it is computationally impractical to analyze the simulation in a long time scale, which would require an excessive number of small time

Table 1 AFM (atomic force microscope) based measurement of SL-20 natural graphite particles approximated by triaxial ellipsoids

particle #	a(μm)	b(μm)	c(μm)	a/c	a/b
1	16.84	13.72	11.89	1.42	1.23
2	4.10	3.64	3.32	1.29	1.16
3	14.13	11.78	10.35	1.37	1.20
4	9.51	6.93	5.75	1.65	1.37
5	7.74	5.48	4.51	1.71	1.41
mean	10.46	8.31	7.16	1.49	1.27
variation	5.07	4.27	3.75	0.16	0.10

Table 2 Geometrical parameters of triaxial ellipsoids used in the simulations

a	b	c
0.0767	0.0604	0.0515

increments. Fortunately, some testing work suggested that the speed of the analysis could be increased substantially without severely degrading the quality of the quasi-static solution. The end result of the slow loading and a somewhat accelerated loading are nearly the same. However, if the loading speed is increased to a point at which inertial effects dominate, the solution tends to localize and the results are quite different from the quasi-static solution. Specifically, when the plate moves sufficiently fast, the upper layers of particles would undergo severe deformation before they transfer the loads to the lower layers. The results would be different from a slow loading case in which a series of stress waves pass through the entire system before the development of any local stresses.

3.2 Simulation Results. Figure 5 is a plot of reactive force applied on the pressing plate as a function of the volume fraction (vf), for both spherical and ellipsoidal particles. The reactive force applied on the plate at the early stage of the simulation was provided solely by the intermittent, dynamic impact of particles against the plate until particles were in intimate contact. After that point, the contribution of the reactive force was primarily a result of local deformation of the particles, and the magnitude of force thus increased significantly. Figure 6 is an enlarged picture of the plot in Fig. 5. In this figure, it is clearly seen that there is a transition region in which the mean amplitude of the pressure increases significantly.

Clearly there *is no* "jamming fraction" for nonrigid particles if material failure is not considered, since the compression process can continue towards vf=100% by deforming the geometrical shape of particles without giving rise to any convergence problems, although the required external load would be much higher once the system becomes "jammed." However, we still retain this term for reference to the jamming fraction for *rigid particles*. From the same figure, we can also observe that a sudden increase of the reactive force on the pressing plate at a certain stage of the compression process (for example, when the volume fraction of the ellipsoidal particles reaches approximately 58% in the absence of friction), implying that the particles are in full contact, reaching the point at which the system is "jammed." This point corresponds to the "jamming fraction" for rigid particles. This is consistent with the above discussion about the two distinct stages in compression. When friction is absent, the systems experience oscillations in the reactive force, implying the rapid changes of contact areas of the interfacial regions between the plate and upper layers of particles when particles are under compression.

The jamming densities for ellipsoids are higher than those for spheres under the same conditions, which is consistent with the results reported in literature [12]. For example, the ellipsoidal system studied here has a "jamming" fraction of 58%, which is slightly higher than that for spheres (55%). In addition, the value of the "jamming" fraction strongly relies on packing history, i.e., the specific method involved in the compression process of a specific system including the initial conditions, boundary conditions,

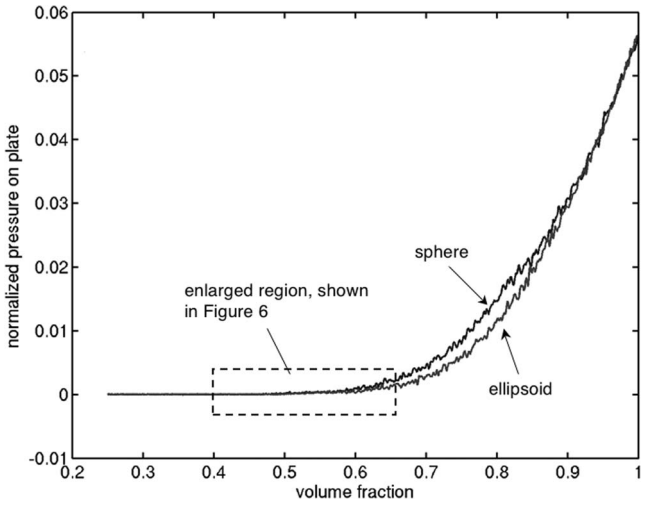

Fig. 5 Reactive force on the pressing plate as a function of volume fraction, for systems of spherical and ellipsoidal particles

compression rate, and the criteria of determining jamming status. In this study, the estimated packing limit 55% for spheres falls inside the range reported in literature [23] but well below the higher bound (64%). This is because "vibration" or "shaking" (as described in a classical experiment [24]) is not used to facilitate the packing in the present study. We believe that the method used in this study can properly represent the compression procedure in many practical applications where vibration is likely not involved.

Simulation results related to the effects of interfacial friction are presented in Fig. 7. Clearly the presence of interfacial friction impedes particle adjustment, and therefore reduces the jamming fraction. This also leads to energy dissipation in the system, causing reduced oscillations in the reactive force. Figure 8 shows the jamming fraction as a function of the friction coefficient, f. In the packing process described in this study, a friction coefficient of 0.3 can reduce the jamming fraction from 58% to 55%, a reduction of 3% in volume fraction. A friction coefficient of 0.5 further reduces the jamming fraction to 52%, a reduction of 6% in volume fraction compared to the no-friction case. The maximum reduction in jamming fraction can be 7% when the friction coefficient is close to 1 and the particles become very "sticky" [25]. No further reduction is observed for greater values of friction coefficient, implying that $f=1$ is sufficient to model "sticky" conditions.

Figure 9 shows the result of Von Mises stress distribution for different friction coefficients. It can be seen that the maximum Von Mises stress increases with volume fraction after close packing and that the existence of friction raises Von Mises stresses significantly. For example, at volume fraction 70%, the Von Mises stresses for $f=0.5$ is almost doubled compared to $f=0.1$.

Figure 10 shows the spheres under compression right after reaching the jamming fraction.

Figure 11 is a close-up picture in the simulation showing severe deformation in the ellipsoidal particles under a high volume fraction 80% (well above the jamming fraction). It can be seen that the boundary shapes of some of the particles are no longer ellipsoidal.

Table 3 Parameters for finite element analysis of particle compression

elastic modulus	density	simulation time	particle number	increment number	friction coeff.
1.0e+3	1.0e-5	1.0e-2	1000	20000~30000	0.5

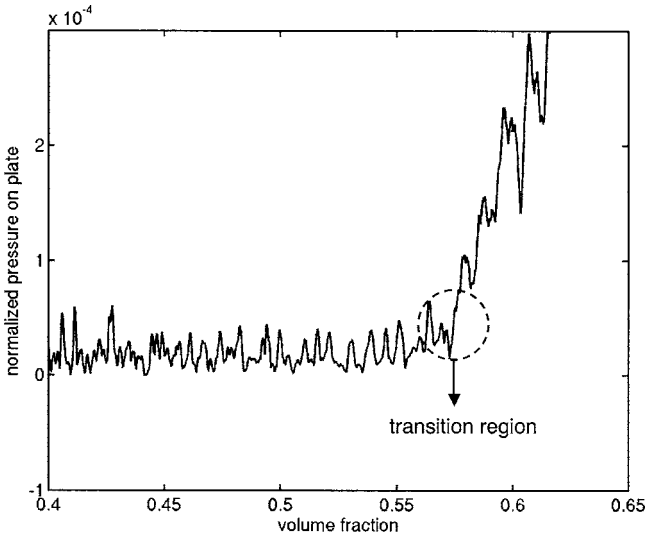

Fig. 6 Close-up picture of Fig. 5 for ellipsoids without friction, for demonstrating the transition between pre-jamming and post-jamming stages during compression

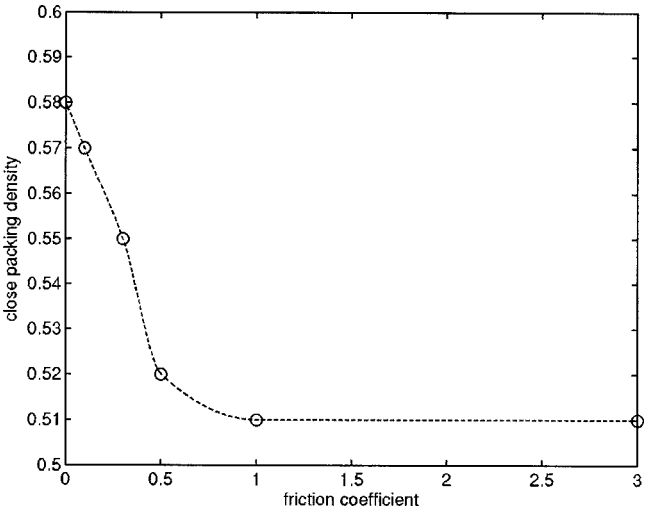

Fig. 8 Jamming fraction as a function of friction coefficient for ellipsoidal particles

4 Discussion

4.1 Theoretical/Modeling Considerations. Although calculation of the maximum packing density can trivially be found as $\pi/\sqrt{12} \approx 90.69\%$ for elliptical and circular disks of the same size [26], it had not been rigorously proven until very recently that the volume fraction of the densest possible arrangement for identical spheres in three dimensions is $\pi/\sqrt{18} \approx 74.05\%$, corresponding to close-packed face-centered cubic (fcc) packing [9]. For random close packing of identical spheres (i.e., amorphous monodisperse sphere packing), however, the volume fraction is lower than that for the crystalline packing. The value could vary [27,28], depending on the experimental or simulation protocol used [6]. In fact, random packings denser than 64% could be achieved, by allowing partial formation of crystallites. For ellipsoidal geometries, studies by Donev et al. [29] revealed that a higher value of packing fraction 77.07% is possible for crystalline arrays of ellipsoids of maximal aspect ratio 3. Recently, the same research group reported via simulation that ellipsoids can also randomly pack more densely [12], up to 68% to 74% in comparison with the maximal density 64% in the random packing for spheres. They also suggested that these values might not be the densest and higher values could exist for aspect ratios other than the ones they used.

4.2 Battery Design Considerations. The curves presented in Figs. 5–8 can be used to guide the material design against the onset of material failure with material properties including bulk modulus and ultimate stress of the particle material, along with an estimated coefficient of friction. In this study, we are interested in the Li-ion anodes, which were comprised of three different types of natural graphite as mentioned in the Introduction. Reports of mechanical properties of natural graphite (including the materials studied here) have varied widely, depending on both initial structure and preparation history. Reported values of elastic modulus from the open literature, for example, range from 4.8 GPa (bulk modulus) [30,31] to 37 GPa (in the direction parallel to the basal planes), and further to 1060 GPa (in the direction parallel to the hexagonal axis) [32]. The ultimate stress of graphite has been found to be sensitive to the processing history of the crystal [32]; reported values range from 0.029 MPa [32] to 131 MPa [30]. The ultimate stress of 131 MPa was derived based on the hardness of 1–2 Mohs [30] scale for graphite and the conversion table of

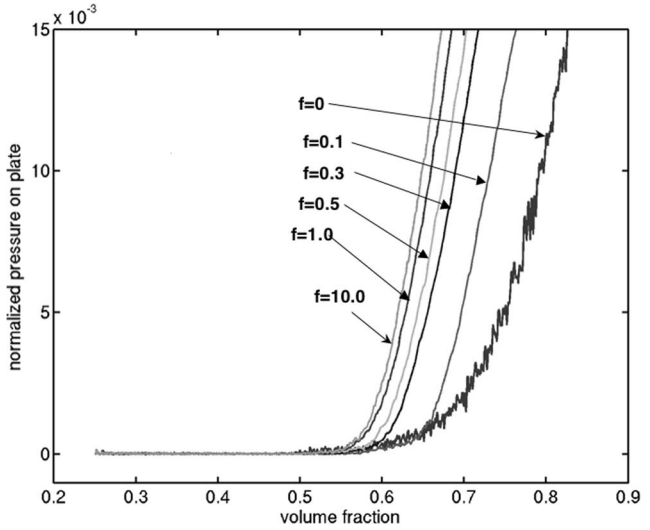

Fig. 7 Reactive force applied on the pressing plate as a function of volume fraction, for systems of ellipsoidal particles, under different friction coefficient ranging from 0 to 10.0

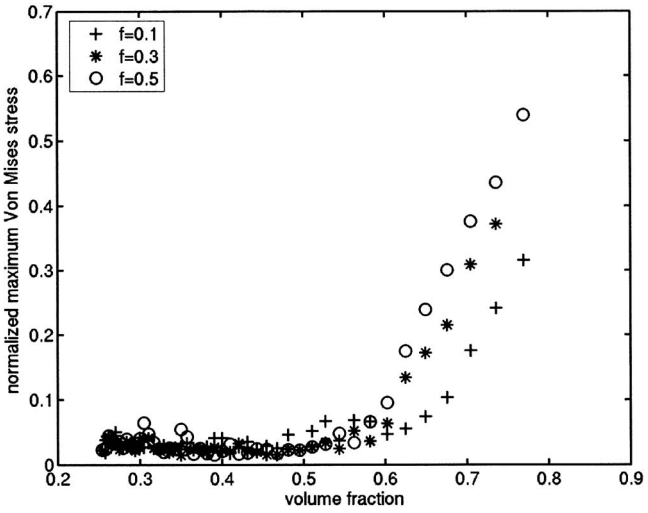

Fig. 9 Maximum internal Von Mises stresses versus volume fraction, for systems of ellipsoidal particles. The stress is normalized against the elastic modulus.

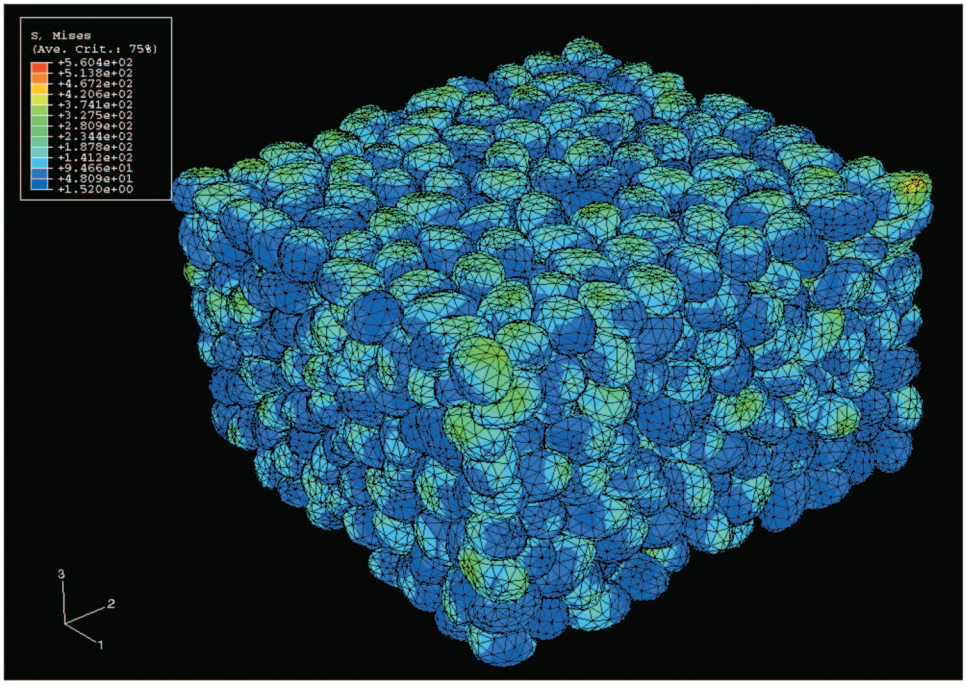

Fig. 10 Von Mises stress distribution in a system of 1000 ellipsoids at friction coefficient 0.5

Mohs scale and a previously reported ultimate stress [33].

In the packed particulate networks studied here, the particles were oriented randomly. Hence, the effective modulus (4.8 GPa) of the graphite networks was averaged over the values along all axes. For the natural graphite (SL-20) electrodes studied here, the volume fraction of particulate networks increased from 68% under an applied pressure of 100 kg/cm^2 (0.01 GPa) to 83% under 200 kg/cm^2 (0.02 GPa). A volume fraction of 90% was found under a pressure of 300 kg/cm^2 (0.03 GPa). Using the lower bound of 4.8 GPa for the modulus of the particles, the normalized pressure in the experiments (applied pressure/modulus =0.01 GPa/4.8 GPa) would be around 2×10^{-3} for the first case (68% volume fraction). Figure 7 shows this case, which has a friction coefficient close to 0.1. Per Fig. 9, the maximum Von Mises stress for a friction coefficient of 0.1 would be approximately 500 MPa (0.1×4.8 GPa), at the same order of magnitude as the upper bound 131 MPa of the ultimate stress reported above. However, when higher pressure, 200 or 300 kg/cm^2, is applied, the maximum Von Mises stress would be at least one order of magnitude higher than the ultimate stress. This suggests possible breakage in graphite particles under the applied pressures 200 or 300 kg/cm^2.

As discussed in [4], the average electronic resistivity of a composite graphite electrode and the average contact resistance at the interface of the composite graphite and the current collector of SL-20 electrodes improved as the applied pressure increased. However, the variance in contact resistance decreased as applied pressure increased from 0 to 200 kg/cm^2 (0.02 GPa). The variance again increased as the applied pressure was increased to 300 kg/cm^2 (0.03 GPa). This result suggests that local failures occur with application of high pressure (>200 kg/cm^2). The simulation results presented in this work are consistent with electronic conductivity experiments reported in [4], that is, the applied pressure above 200 kg/cm^2 (0.02 GPa) can be detrimental to the SL-20 electrode.

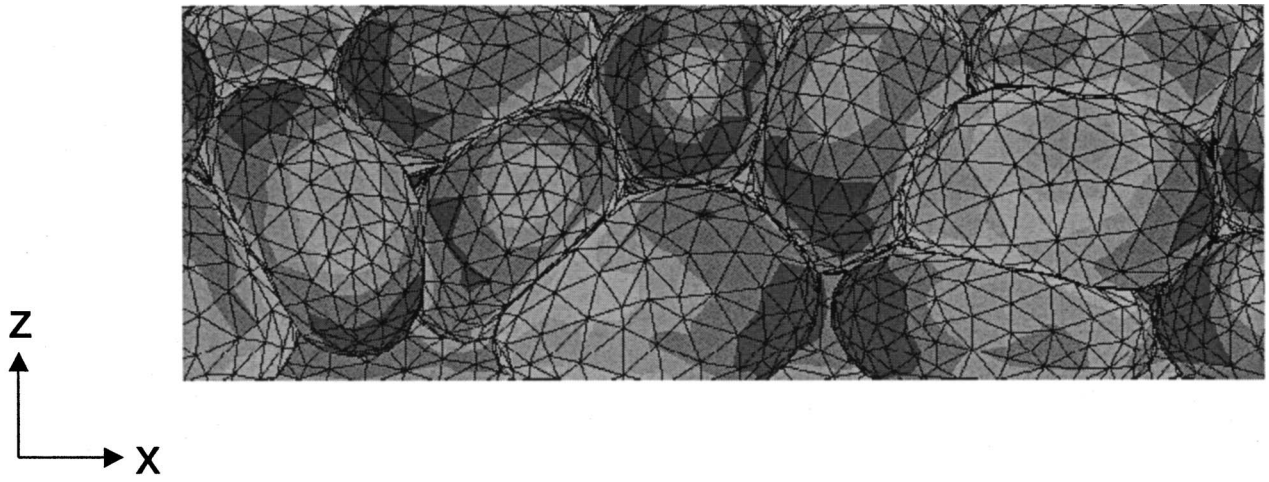

Fig. 11 Severe local deformation of ellipsoids can be observed at volume fraction 90%. Friction coefficient 0.5.

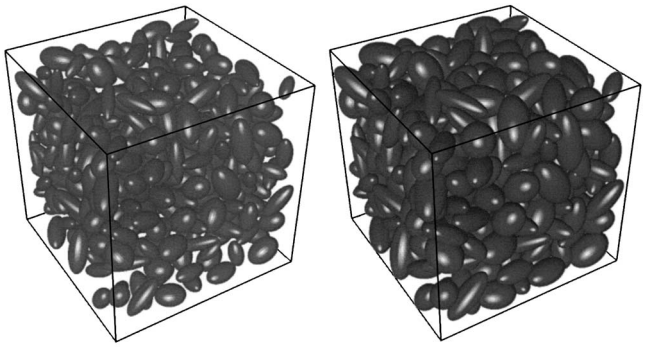

(*a*) (*b*)

Fig. 12 Computer generation of a polydisperse particulate system comprised of impermeable ellipsoids (*a*) with varied aspect ratio and no coating and (*b*) with varied aspect ratio and coating layers. Note in (*b*) that the coating layers are exaggerated: their thickness is 40% of the mean diameter of the hard cores.

5 Conclusions and Future Work

We presented a method to simulate the compression of packed particulate systems in graphitic Li-ion anodes and investigated the quantitative relations among the interfacial friction, packing limit, applied pressure, and maximum internal stresses. Simulation results were compared with experiments, showing that the friction coefficient in the system is close to 0.1 and that applied pressure above 200 kg/cm^2 (200 MPa) can damage the materials in SL-20 electrodes.

We also conclude that the use of maximum jamming fractions to assess likely configuration of mixtures is unrealistic at best, in real manufacturing processes. Particles changed both their overall shapes and relative orientations during deformation sufficient to alter the composite properties: indeed, it is the alteration of properties that motivates post-processing at all. Thus, consideration of material properties, or their estimation post facto, using inverse techniques, is clearly merited in composites having volume fractions of particles near percolation onset.

For compression of deformable materials, the internal stress results from (1) dynamic impact caused by the rapid motion of the pressing plate and (2) post-packing deformation of the particulate system, as discussed earlier. The presence of interfacial friction reduces relative motion among particles, causing localized deformation at the interfaces. This can result in faster increase of Von Mises stresses for a system with a high friction coefficient compared to the low friction cases, as seen in Fig. 9.

Although the technique developed in this study was based on a monodisperse system of simple elastic material properties, it can be readily extended to more complicated systems. For example, Fig. 12(*a*) shows a system of ellipsoids of varied aspect ratio with a normal distribution of mean 2.0 and standard deviation 1.0. A system of ellipsoids of hard core covered by a thin layer of penetrable coating materials can also be generated as shown in Fig. 12(*b*) via uniformly dilating the particle along the axial directions. Different material properties will be assigned to the core and coating layer in the finite element model accordingly. These models can be considered as a natural extension of the method developed in this study and will be incorporated in our future work.

Acknowledgment

Support for this work provided by the W. M. Keck Foundation, DARPA, and ONR through the Synthetic Multifunctional Materials (SMFM) Program (Dr. Leo Christodoulou and Dr. Steve Fishman, Program Monitors) is gratefully acknowledged. Support from an NSF PECASE (Sastry) and a supercomputing cluster, a gift of Sun Microsystems to the authors, are also acknowledged. We appreciate the generous support of our sponsors.

References

[1] Maleki, H., Selman, J. R., Dinwiddie, R. B., and Wang, H., 2001, "High Thermal Conductivity Negative Electrode Material for Lithium-Ion Batteries," J. Power Sources, **94**, pp. 26–35.
[2] Striebel, K. A., Sierra, A, Shim, J., Wang, C.-W., and Sastry, A. M., 2004, "The Effect of Compression on Natural Graphite Anode Performance and Matrix Conductivity," J. Power Sources, **134**(2), pp. 241–251.
[3] Gnanaraj, J. S., Cohen, Y. S., Levi, M. D., and Aurbach, D., 2001, "The Effect of Pressure on the Electroanalytical Response of Graphite Anodes, and $LiCoO_2$ Cathodes for Li-ion Batteries," J. Electroanal. Chem., **516**(1-2), pp. 89–102.
[4] Wang, C.-W., Yi, Y.-B., Sastry, A. M., Shim, J., and Striebel, K. A., 2004, "Particle Compression and Conductivity in Li-ion Anodes with Graphite Additives," J. Electrochem. Soc., **151**(9), pp. 1489–1498.
[5] Kansal, A. R., Torquato, S., and Stillinger, F. H., 2002, "Computer Generation of Dense Polydisperse Sphere Packings," J. Chem. Phys., **117**, pp. 8212–8218.
[6] Torquato, S., Truskett, T. M., and Debenedetti, P. G., 2000, "Is Random Close Packing of Spheres Well Defined?" Phys. Rev. Lett., **84**, pp. 2064–2067.
[7] Torquato, S, 2000, "Modeling of Physical Properties of Composite Materials," Int. J. Solids Struct., **37**(1-2), pp. 411–422.
[8] Torquato, S, 1985, "Effective Electrical-Conductivity of 2-Phase Disordered Composite Media," J. Appl. Phys., **58**(10), pp. 3790–3797.
[9] Hales, T. C., 1997, "Sphere Packings I," Discrete Comput. Geom., **17**(1), pp. 1–51.
[10] Yi, Y.-B., Sastry, A. M., and Philbert, M. A., 2006, "Three-dimensional Reconstruction of Cell Boundaries and Interior Organelles from Confocal Microscopy, Using a Combined Delaunay Tesselation/Stochastic Placement Scheme," Journal of Computational Physics, in review.
[11] Lubachevsky, B. D., and Stillinger, F. H., 1990, "Geometric-Properties of Random Disk Packings," J. Stat. Phys., **60**, pp. 561–583.
[12] Donev, A., Cisse, I., Sachs, D., Variano, E., Stillinger, F. H., Connelly, R., Torquato, S., and Chaikin, P. M., 2004, "Improving the Density of Jammed Disordered Packings using Ellipsoids," Science, **303**, pp. 990–993.
[13] Jodrey, W. S., and Tory, E. M., 1985, "Computer Simulation of Close Random Packing of Equal Spheres," Phys. Rev. A, **32**, pp. 2347–2351.
[14] Bezrukov, A., Bargiel, M., and Stoyan, D., 2002, "Statistical Analysis of Simulated Random Packings of Spheres," Part. Part. Syst. Charact., **19**, pp. 111–118.
[15] Williams, S. R., and Philipse, A. P., 2003, "Random Packings of Spheres and Spherocylinders Simulated by Mechanical Contraction," Phys. Rev. E, **67**, p. 051301.
[16] Vieillard-Baron, J., 1972, "Phase Transitions of the Classical Hard-Ellipse System," J. Chem. Phys., **56**, pp. 4729–4744.
[17] Donev, A., Torquato, S., and Stillinger, F. H., 2005, "Neighbor List Collision-Driven Molecular Dynamics Simulation for Nonspherical Particles: I. Algorithmic Details II. Applications to Ellipsoids," J. Comput. Phys., **202**, pp. 409–416.
[18] ABAQUS/EXPLICIT User's Manual version 6.3, Hibbitt, Karlsson & Sorensen Inc., 2002.
[19] Shim, J., and Striebel, K. A., 2004, "The Dependence of Natural Graphite Anode Performance on Electrode Density," J. Power Sources, **130**, pp. 247–253.
[20] Yoo, M., Frank, C. W., and Mori, S., 2003, "Interaction of Poly(vinylidene fluoride) with Graphite Particles. 1. Surface Morphology of a Composite Film and its Relation to Processing Parameters," Chem. Mater., **15**, pp. 850–861.
[21] http://www.matweb.com (2005).
[22] Yi, Y.-B., Wang, C.-W., and Sastry, A. M., 2004, "Two-Dimensional versus Three-Dimensional Clustering and Percolation in Fields of Overlapping Ellipsoids," J. Electrochem. Soc., **151**, pp. A1292–A1300.
[23] Onoda, G. Y., and Liniger, E. G., 1990, "Random Loose Packings of Uniform Spheres and the Dilatancy Onset," Phys. Rev. Lett., **64**, pp. 2727–2730.
[24] Scott, G. D., and Kilgour, D. M., 1969, "Density of Random Close Packing of Spheres," J. Appl. Phys., J. Phys. D, **2**(6), pp. 863–866.
[25] Zinchenko, A., 1994, "Algorithm for Random Close Packing of Spheres with Periodic Boundary Conditions," J. Comput. Phys., **114**, pp. 298–307.
[26] Pach, J., and Agarwal, P. K., 1995, *Combinatorial Geometry*, Wiley-Interscience, New York.
[27] Kansal, A. R., Torquato, S., and Stillinger, F. H., 2002, "Diversity of Order and Densities in Jammed Hard-Particle Packings," Phys. Rev. E, **66**, p. 041109, Part 1.
[28] Donev, A., Torquato, S., Stillinger, F. H., and Connelly, R., 2004, "Jamming in Hard Sphere and Disk Packings," J. Appl. Phys., **95**, pp. 989–999.
[29] Donev, A., Stillinger, F. H., Chaikin, P. M., and Torquato, S., 2004, "Unusually Dense Crystal Packings of Ellipsoids," Phys. Rev. Lett., **92**, p. 255506.
[30] http://www.matweb.com (2004).
[31] http://www.goodfellow.com/csp/active/static/A/C_00.HTML (2004).
[32] Kelly, B. T., 1981, *Physics of Graphite*, Applied Science Publishers, London.
[33] Dowling, N. E., 1999, *Mechanical Behavior of Materials: Engineering Methods for Deformation, Fracture, and Fatigue*, 2nd ed., Prentice Hall, Upper Saddle River, NJ.